Acta Crystallographica Section D
Biological Crystallography
ISSN 0907-4449

Structures of the *Porphyromonas gingivalis* OxyR regulatory domain explain differences in expression of the OxyR regulon in *Escherichia coli* and *P. gingivalis*

David V. Svintradze,[a,b]‡ Darrell L. Peterson,[b,c] Evys A. Collazo-Santiago,[a] Janina P. Lewis[a] and H. Tonie Wright[b,c]*

[a]OCMB Philips Institute, School of Dentistry, Virginia Commonwealth University, Richmond, VA 23298-0566, USA, [b]Institute for Structural Biology and Drug Discovery of Virginia Commonwealth University, Virginia Commonwealth University, Richmond, VA 23219-1540, USA, and [c]Department of Biochemistry and Molecular Biology, Virginia Commonwealth University, Richmond, VA 23298-0614, USA

‡ Present address: Department of Physics, Tbilisi State University, 0128 Tbilisi, Republic of Georgia.

Correspondence e-mail: xrdproc@vcu.edu

Received 9 January 2013
Accepted 15 July 2013

PDB References: *P. gingivalis* OxyR RD, oxidized, 3ho7; mutant, 3t22; reduced, 3uki

OxyR transcriptionally regulates *Escherichia coli* oxidative stress response genes through a reversibly reducible cysteine disulfide biosensor of cellular redox status. Structural changes induced by redox changes in these cysteines are conformationally transmitted to the dimer subunit interfaces, which alters dimer and tetramer interactions with DNA. In contrast to *E. coli* OxyR regulatory-domain structures, crystal structures of *Porphyromonas gingivalis* OxyR regulatory domains show minimal differences in dimer configuration on changes in cysteine disulfide redox status. This locked configuration of the *P. gingivalis* OxyR regulatory-domain dimer closely resembles the oxidized (activating) form of the *E. coli* OxyR regulatory-domain dimer. It correlates with the observed constitutive activation of some oxidative stress genes in *P. gingivalis* and is attributable to a single amino-acid insertion in *P. gingivalis* OxyR relative to *E. coli* OxyR. Modelling of full-length *P. gingivalis*, *E. coli* and *Neisseria meningitidis* OxyR–DNA complexes predicts different modes of DNA binding for the reduced and oxidized forms of each.

1. Introduction

Bacteria have evolved to express a number of enzymes and proteins that orchestrate protective responses to damaging reactive oxygen species (ROS) such as superoxide (O_2^-), peroxides, oxides of nitrogen and hydroxyl radicals, which are generated both endogenously as by-products of aerobic metabolism and exogenously (Imlay, 2002, 2008). These enzymes include superoxide dismutase, catalase, peroxidase and a number of other proteins that directly and indirectly mitigate the damaging activities and effects of ROS.

The transcriptional regulation of the oxidative stress response (OSR) has been most thoroughly investigated in *Escherichia coli*, a facultative anaerobe whose OxyR regulon controls the expression of a number of OSR genes (Zheng *et al.*, 2001). OxyR is a member of the LysR family of transcriptional regulatory proteins, which consist of an amino-terminal DNA-binding domain (DBD) of about 80 amino acids and a carboxyl-terminal regulatory domain (RD) that acts as a sensor and switch (Antelmann & Helmann, 2011). Reduced *E. coli* OxyR is in the 'open' form and oxidized *E. coli* OxyR is in the 'closed' form (Maddocks & Oyston, 2008), the reduced form being more stable thermodynamically than the oxidized form (Lee *et al.*, 2004).

E. coli OxyR is a ROS (H_2O_2) sensor and responds to H_2O_2 oxidative stress through the reversible oxidation of two cysteines (Cys199 and Cys208) in its RD to form a disulfide bridge (Storz & Imlay, 1999; Ryu, 2012). In its oxidized form *E. coli* OxyR is a transcriptional activator of OSR genes.

It also autorepresses its own transcription and activates divergent transcription of OxyS from the same promoter-binding site that represses OxyR transcription. Reduced *E. coli* OxyR tetramer also represses OxyR transcription and that of several other genes (Zheng *et al.*, 2001), but does not bind the promoter regions of other OSR genes (*ahpC*, *katG*, *gorA* and *dps*). The oxidized (activated) OxyR tetramer binds to two tandem bipartite DNA promoter sites in four successive DNA major grooves to activate transcription (Toledano *et al.*, 1994). Reduced *E. coli* OxyR binds to a longer sequence in the OxyRS promoter than oxidized OxyR, with the two reduced promoter-bound homodimers being separated by one extra turn of DNA duplex relative to the binding of oxidized OxyR tetramer (Toledano *et al.*, 1994). The extended promoter-binding site of reduced *E. coli* OxyR appears to bend the promoter DNA at its central turn, which results in repression.

The crystal structures of *E. coli* OxyR RD in its oxidized and reduced forms showed that the conformation of the switch loop region from Cys199 to Cys208 is dependent on the redox status of the cysteines (Choi *et al.*, 2001). Oxidation/reduction of this disulfide bridge and the attendant conformational changes in the intervening disulfide loop cause a change in the local monomer conformation which propagates to the dimer interface and induces changes in dimer and tetramer quaternary interactions. Modeling of the full-length *E. coli* OxyR and its complex with DNA led to the hypothesis that the redox-induced changes in quaternary interactions of the *E. coli* OxyR RD trigger reorientation of the amino-terminal DBDs of the tetramer and change their promoter-binding mode and regulatory activity (Choi *et al.*, 2001).

There is evidence that the *E. coli* OxyR regulon (Zheng *et al.*, 2001) differs from that of *P. gingivalis* (Diaz *et al.*, 2006). H_2O_2 exposure in *E. coli* leads to strong (greater than tenfold) up-regulation of 30 genes, of which at least six (*dps*, *katG*, *grxA*, *ahpF*, *trxC* and *ahpC*) have functions directly linked to OSR. Other OSR genes in the OxyR regulon (*gorA*, *grxA* and *fur*) are not strongly induced by H_2O_2. In *P. gingivalis*, H_2O_2 stress leads to weak (less then fivefold) induction of nine genes, none of which are directly associated with the OSR (Diaz *et al.*, 2006). Some of the OxyR-regulated genes that can be linked to the OSR in *P. gingivalis* (*ahpc*, *dps*, *ahpf*, *sod*, *ftn* and *thioredoxin*) are constitutively activated (Diaz *et al.*, 2006) and weakly or not induced by H_2O_2 (Diaz *et al.*, 2006; Ohara *et al.*, 2006; Wu *et al.*, 2008). *katG* is absent in *P. gingivalis* and *sod* is in the SoxRS regulon in *E. coli*. OxyR contributes to the aerotolerance of *P. gingivalis* through modest induction of *sodA* and *ahpC* (Meuric *et al.*, 2008; Ohara *et al.*, 2006; Wu *et al.*, 2008) and *ftn* and *tpx*, but does not appear to function as an H_2O_2 sensor. It has been proposed that anaerobes survive transient exposure to oxidative stress conditions through the constitutive activation by OxyR of a distinct panel of OSR genes (Fareleira *et al.*, 2003). In *P. gingivalis* (Diaz *et al.*, 2006) and *Tannerella forsythia* (Honma *et al.*, 2009) OxyR constitutively activates OSR genes, but only some of these are the same as the OSR-induced genes in *E. coli*. The constitutive activation of OSR genes in *P. gingivalis* has been hypothesized to result from OxyR being locked in its oxidized (activator) conformation (Diaz *et al.*, 2006; Honma *et al.*, 2009).

The crystal structures of the oxidized and C199S mutant (equivalent to the reduced) forms of *P. gingivalis* OxyR RD confirm this hypothesis and provide a structural basis for constitutive activation of OxyR-regulated OSR genes in *P. gingivalis*. Oxidation/reduction of the Cys199 and Cys208 cysteines in *P. gingivalis* OxyR RD induces only very limited secondary- and tertiary-structural changes in the same localized region as observed in *E. coli* OxyR RD. However, these changes differ from those observed in *E. coli* OxyR RD and result in only minor changes in the dimer interface of *P. gingivalis* OxyR RD on cysteine disulfide oxidation/reduction and no change in the disposition of the monomers of the 'locked' dimer.

What is the origin of the differences in structural properties of these two closely similar tertiary structures? Comparison of bacterial OxyR amino-acid sequences shows that a subset of sequences, including *P. gingivalis* OxyR, carry a short variable-length sequence insertion at residue 215 relative to the *E. coli* OxyR sequence. In *P. gingivalis* OxyR RD structures, the single Arg insertion after residue 215 clearly alters the local conformation relative to *E. coli* OxyR RD and thereby affects the monomer–monomer interface of the dimer. The crystal structure of reduced OxyR RD from *N. meningitidis*, which has a five-residue insert at residue 215, also supports a critical role for the 215 insert in determining OxyR structure and function. This structure and model building of the oxidized *N. meningitidis* OxyR RD structure suggest that this OxyR RD is stabilized in the reduced form. We hypothesize that it also does not undergo quaternary structure transitions like those inferred for *E. coli* OxyR.

Correlation of the residue 215 insertion with a more stable dimer configuration of oxidized *P. gingivalis* and reduced *N. meningitidis* dimers leads us to the hypothesis that insertion at this site in the sequence is a determinant of OxyR regulatory functions specific to different bacterial species. In the case of *P. gingivalis* OxyR, a single amino-acid insertion confers constitutive activation of some oxidative-stress genes. Models of full-length oxidized and reduced *P. gingivalis* OxyR bound to DNA show a pattern of possible bound OxyR oligomer structures distinct from those inferred for the full-length *E. coli* OxyR RD. This is consistent with the different regulatory responses observed for these two bacterial species. Insertions at residue 215 in OxyRs of other bacterial species, such as *N. meningitidis*, may differentially alter dimer stability and thereby affect the nature of gene regulation and possibly also the gene complement of their OxyR regulons.

2. Experimental procedures

2.1. Protein preparation

P. gingivalis full-length wild-type OxyR (W83 strain, LANL Gene ID PG0242), OxyR RD (residues 90–308), C199S OxyR RD and ΔR215 OxyR RD were cloned into a pET30a plasmid (Novagen) carrying a carboxyl-terminal His tag. The C199S

construct was made by mutagenizing wild-type OxyR RD using the QuikChange site-directed mutagenesis kit (Stratagene) and the sequences were confirmed (VCU Nucleic Acids Core Facility). Proteins were expressed in *E. coli* BL21(DE3) cells grown in autoinduction LB medium with kanamycin. After 18 h of growth, the cells were collected by centrifugation, suspended in 25 m*M* Tris–HCl pH 8.0, 0.3 *M* sodium chloride, 20 m*M* imidazole and disrupted by a single passage through an Avestin C3 Emulsiflex high-pressure homogenizer at a pressure of 138 MPa. The lysate was clarified by centrifugation for 30 min at 15 000*g* and the clear supernatant was bound to a Bio-Rad IMAC affinity column and washed with the same buffer; the protein was then eluted using either 100 m*M* EDTA or an imidazole gradient in the same buffer. The eluted protein was precipitated by the addition of solid ammonium sulfate to 50% saturation and the precipitate was collected by centrifugation. Resuspended full-length OxyR was dialyzed *versus* 10 m*M* Tris–HCl pH 9, 0.1 *M* sodium chloride, the wild-type OxyR RD was dialyzed *versus* 25 *M* Tris–HCl pH 8.0 and the C199S OxyR RD mutant was dialyzed *versus* 25 *M* Tris–HCl pH 8.0, 0.5 *M* NaCl, 5 m*M* β-mercaptoethanol. Some batches of wild-type and C199S OxyR RD were further purified on an S100 (Sephacryl) sizing column, dialyzed *versus* 25 m*M* Tris pH 8.0, 0.5 *M* NaCl and concentrated to 3.9 and 7.5 mg ml^{-1}, respectively. OxyR expressed from the full-length gene ran with a molecular weight of about 25 kDa on SDS–PAGE, indicating that cleavage had occurred between the amino-terminal DNA-binding domain and the regulatory domain during preparation.

2.2. Crystallization, heavy-atom soaks and data collection

P. gingivalis OxyR RD (from the preparation of full-length expressed OxyR) was crystallized by hanging-drop vapor diffusion at 291 K by mixing a 2.5 µl aliquot of protein solution (3.9 mg ml^{-1}) with 3.75 µl reservoir solution consisting of 12% PEG 8K, 8% ethylene glycol, 0.1 *M* HEPES pH 7.5. Crystals appeared in 5 d and grew to 0.5 mm in two weeks. The lattice was determined to be *P*1, with unit-cell parameters a = 55.88, b = 55.12, c = 56.81 Å, α = 110.65, β = 102.81, γ = 114.59° and two molecules per asymmetric unit. Crystals in their growth drops were soaked with heavy atoms for 4 d at 291 K by direct addition to the drops of 2.5 µl of heavy atom in precipitant solution. One solution consisted of 1 m*M* ethylmercurithiosalicylate. The other heavy-atom solution was made by combining 2 µl of a 1 m*M* solution of ethylmercurithiosalicylate with a solution consisting of 10 µl each of spun supernatants of saturated solutions of the following compounds: dimercury acetate, *p*-chloromercuribenzoic acid, 2,5-dichloromercurifuran, mersalyl, *o*-chloromercuriphenol, phenylmercury salicylate and phenylmercuriboronic acid.

The OxyR RD C199S mutant was crystallized at 293 K by mixing a 2 µl aliquot of the OxyR RD mutant (15 mg ml^{-1}) in 500 m*M* NaCl, 25 m*M* Tris pH 8.0, 5 m*M* β-mercaptoethanol in sitting drops with the same volume of reservoir solution consisting of 30% PEG 3000, 0.1 *M* CHES pH 9.5. Crystals appeared in three weeks and grew to a size comparable to the oxidized form within a month. These crystals also belonged to space group *P*1, but with unit-cell parameters a = 56.209, b = 64.356, c = 81.312 Å, α = 111.75, β = 90.56, γ = 111.24°, consistent with four monomers per unit cell. Reduced OxyR RD was crystallized from sitting drops consisting of 2 µl protein solution (5 mg ml^{-1}) in 25 m*M* Tris pH 8, 19 m*M* NaCl, 5 m*M* β-mercaptoethanol and 2 µl reservoir solution consisting of 0.2 *M* $LiSO_4$, 20% PEG 3350 pH 6.0 at room temperature. Crystals appeared in one week; they grew to 0.5 mm in two weeks and belonged to space group $P2_12_12_1$, with unit-cell parameters a = 63.236, b = 82.814, c = 170.484 Å.

A full sphere of X-ray intensity data was collected for native and the two heavy-atom soaks of oxidized OxyR RD and for the OxyR RD C199S mutant without further cryoprotection. Crystals of reduced OxyR RD were cryoprotected for 1–2 min in reservoir solution with glycerol added to 20%(*v*/*v*) and a half sphere of data was collected. Data were collected at 100 K on an R-AXIS IV^{++} image-plate detector using a Rigaku MicroMax-007 X-ray source equipped with MSC VariMax confocal optics operating at 40 kV and 20 mA. Data were processed and scaled with *d*TREK*, and MIRAS phases were obtained using *PHENIX* (Adams *et al.*, 2002). The OxyR RD C199S mutant structure was determined by molecular replacement with oxidized OxyR RD monomer as the search model. Phases were refined in alternating cycles of manual fitting into σ_A-weighted $2mF_o - DF_c$ maps using *Coot* (Emsley & Cowtan, 2004) and computational refinement in *REFMAC5* (Murshudov *et al.*, 2011). Data-collection and refinement statistics are summarized in Table 1.

2.3. Structure determination and refinement

Attempts to solve the oxidized *P. gingivalis* OxyR RD structure by molecular replacement using *E. coli* OxyR RD templates (PDB entries 1i6a and 1i69; Choi *et al.*, 2001) were unsuccessful. Heavy-atom soaks gave four heavy-atom sites from difference Patterson maps using *PHENIX AutoSol* (Adams *et al.*, 2010) and were used to calculate initial phases, which had an overall figure of merit (FOM) of 0.58. The initial electron-density map calculated using these MIRAS phases showed clear solvent boundaries and secondary-structural features and after autobuilding in *PHENIX* (FOM of 0.84) permitted tracing of the entire backbone except for the amino-terminal nine residues of the oxidized *P. gingivalis* OxyR RD. The final electron-density map was obtained after refinement of phases in *REFMAC* (FOM = 0.92). The structure of the oxidized *P. gingivalis* OxyR RD monomer was used as a search model to determine the reduced and C199S mutant OxyR RD structures by molecular replacement. The structures were refined in *PHENIX*, including simulated annealing, and checked in OMIT maps. The low-resolution reduced OxyR RD structure was refined to 4.15 Å resolution using simulated annealing and TLS with a single group. Manual checking and minor editing of the structure were performed and positional refinement with secondary-structure constraints and program-determined TLS groups was run. The

Table 1
Data-collection and refinement statistics for oxidized, C199S mutant and reduced *P. gingivalis* OxyR RD crystals.

Values in parentheses are for the highest resolution shell.

	Oxidized	HG1	HG2	C199S mutant	Reduced
Data collection					
Space group	*P*1	*P*1	*P*1	*P*1	$P2_12_12_1$
Unit-cell parameters					
a (Å)	55.88	55.74	55.19	56.209	63.236
b (Å)	55.12	55.79	55.20	64.356	82.814
c (Å)	56.81	56.75	56.38	81.312	170.484
α (°)	110.65	110.87	110.65	111.75	90.0
β (°)	102.81	102.43	101.61	90.56	90.0
γ (°)	114.59	114.71	115.72	111.24	90.0
Resolution (Å)	26.94–1.58 (1.62–1.58)	27.68–2.20 (2.28–2.20)	27.56–2.20 (2.28–2.20)	18.36–2.20 (2.28–2.20)	33.95–3.50 (3.68–3.50)
$R_{\rm merge}$	0.032 (0.324)	0.048 (0.202)	0.041 (0.131)	0.082 (0.490)	0.289 (0.676)
$\langle I/\sigma(I)\rangle$	19.9 (3.7)	16.7 (4.6)	12.2 (4.9)	8.7 (2.0)	2.4 (0.8)
Completeness (%)	83.56 (41.8)	93.2 (90.0)	95.8 (93.5)	91.6 (90.5)	87.85 (85.8)
Multiplicity	3.92 (3.93)	3.69 (3.68)	1.96 (1.96)	3.530 (3.32)	2.91 (2.97)
Anomalous signal	—	0.6366	0.3650	—	—
Refinement					
Resolution (Å)	1.58			2.20	4.15
No. of reflections	57380			44680	6878
$R_{\rm work}/R_{\rm free}$	0.219/0.244			0.234/0.274	0.31/0.40
No. of atoms					
Total	3952			7118	6606
Protein	3534			6725	6606
Water	418			393	—
B factors (Å^2)					
Protein	23.70			38.70	104.6
Water	28.203			40.473	—
R.m.s. deviations					
Bond lengths (Å)	0.003			0.009	0.007
Bond angles (°)	0.648			1.205	1.33

final model (R and $R_{\rm free}$ of 0.31 and 0.40, respectively) had 4% Ramachandran distribution outliers.

2.4. Homology modeling

Oxidized *N. meningitidis* OxyR RD and full-length *P. gingivalis* and *N. meningitidis* OxyR monomers and dimers were modeled using the *SWISS-MODEL* automated homology-modeling server (Arnold *et al.*, 2006; Kiefer *et al.*, 2009; Peitsch, 1995) with the DBD of the full-length LysR transcriptional regulator CbnR (PDB entry 1iz1; Muraoka *et al.*, 2003) as a template. The linking segments between the modeled DBD and RD were regularized by refinement in *Coot*. Clashes between side chains that required no major conformational changes in the main chain were adjusted and re-regularized, while clashes with main chain or that required large alterations in conformation were scored as impossible structures. All available full-length LysR templates [CbnR (PDB entries 1iz1 and 1ixc; Muraoka *et al.*, 2003); TtgV (PDB entries 2xrn and 2xro; Lu *et al.*, 2010); TsaR (PDB entry 3fxq; Monferrer *et al.*, 2010); PA01 (PDB entry 3fzv; Midwest Center for Structural Genomics, unpublished work); and Pa0477 (PDB entry 2esn; Midwest Center for Structural Genomics, unpublished work)] were tested and analyzed for all possible dimer conformations of *P. gingivalis*, *E. coli* and *N. meningitidis* OxyR dimers.

The full-length LysR-type transcriptional regulator CbnR (PDB entry 1iz1) is the only available closed tetramer template for reduced *P. gingivalis* OxyR and was used as a template for modeling reduced and oxidized full-length *P. gingivalis* and *N. meningitidis* OxyR. Plausible OxyR tetramers were modeled as the DNA complex using the DNA structure from the TtgV crystal structure (PDB entry 2xro) as a template.

3. Results

3.1. Description of overall structures

Crystallization attempts with full-length *P. gingivalis* OxyR gave crystals that consisted of only the OxyR RD, the amino-terminal DNA-binding domain having been proteolytically cleaved off during preparation. Amino-terminal analysis of the protein solution from the drop in which crystals formed gave the sequence IIEEE, corresponding to residues 81–85 of full-length *P. gingivalis* OxyR and confirming cleavage in the connector region between the DNA-binding and regulatory domains. The structure of this air-oxidized *P. gingivalis* OxyR RD dimer was determined with phases obtained by MIRAS and refined with data to 1.58 Å resolution (Table 1). Complete electron density (Fig. 1) was traced for all residues (90–309 of both monomers) except for the nine residues at the amino-terminus, which were disordered. Reduced and C199S mutant *P. gingivalis* OxyR RD (residues 90–308) were expressed in truncated form and crystallized in the presence of 5 m*M* β-mercaptoethanol. Their structures were determined to resolutions of 4.15 and 2.2 Å, respectively, by molecular replacement using the oxidized *P. gingivalis* OxyR RD structure as a search model. The complete polypeptide chain was traced for the C199S mutant (Figs. 2*a*, 2*c* and 2*e*) and disulfide-reduced (Supplementary Fig. S1[1]) structures from residues 90 to 308, except for the 211–218 segment, which was disordered. The structures of the oxidized and C199S forms were refined by *REFMAC* and *PHENIX* refinement, respectively (Table 1).

The folds of the oxidized and reduced *P. gingivalis* OxyR RD monomers are closely similar to each other and to those of oxidized and C199S *E. coli* OxyR RD and of reduced

[1] Supplementary material has been deposited in the IUCr electronic archive (Reference: CB5032). Services for accessing this material are described at the back of the journal.

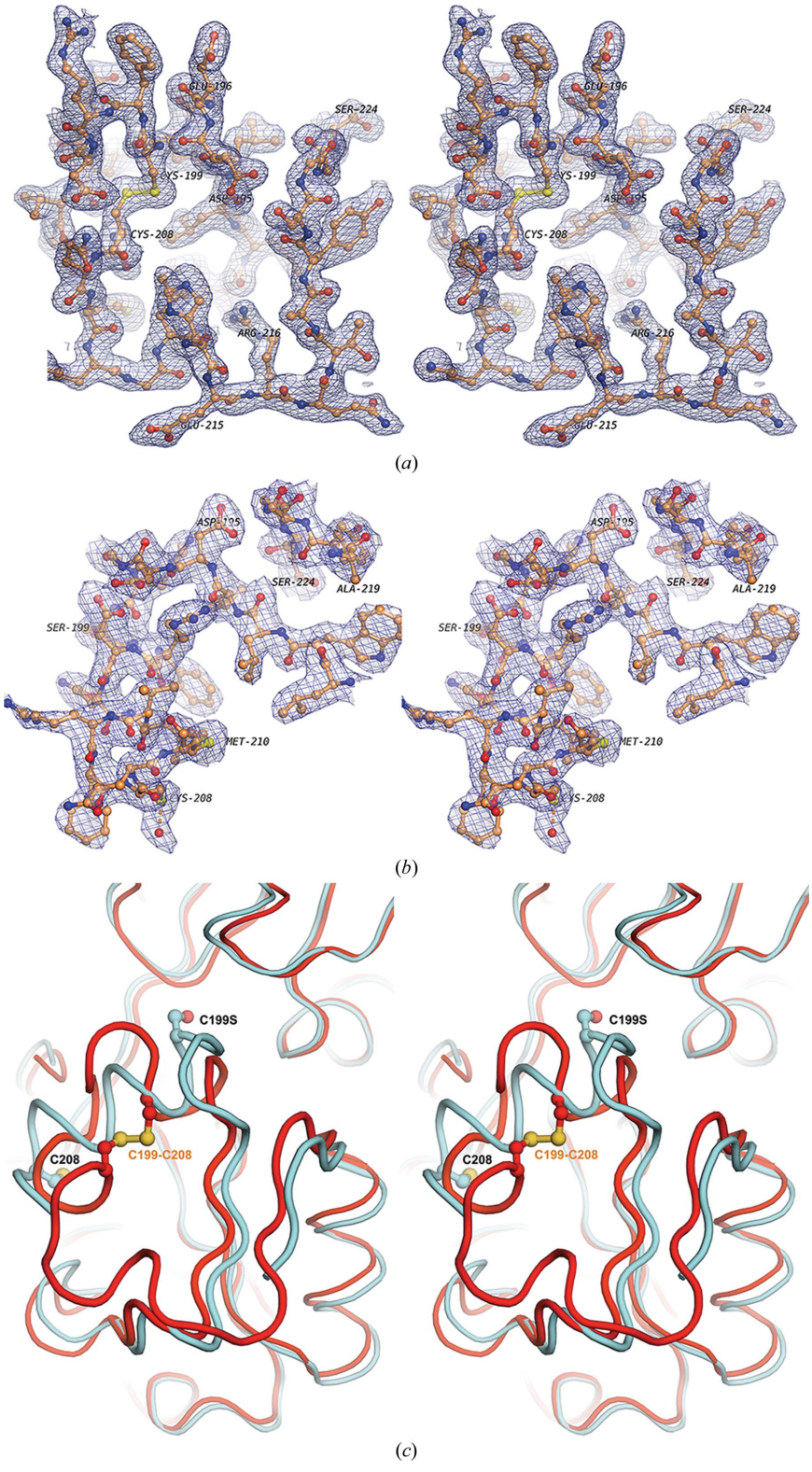

Figure 1
Stereoview of representative $2F_o - F_c$ electron density for the disulfide loop and downstream region of (*a*) oxidized and (*b*) C199S mutant *P. gingivalis* OxyR contoured at 1σ. (*c*) Stereoview of the backbone trace of the disulfide loop of the C199S (cyan) and oxidized wild-type (red) OxyR RD monomer backbone folds. The two structures are aligned by superposition of the C^{α} atoms of those residues that fall below a cutoff of 2.0 Å resolution in the unfiltered fit. The r.m.s.d. values are 1.71 Å without rejection and 0.749 Å for the alignment of 186 residues, which excluded residues 186–226. The redox-active cysteines are shown in ball-and-stick representation.

N. meningitides OxyR RD. They consist of two domains (α/β) linked by an antiparallel pair of β-strands (155–169 and 264–274). The α domain consists primarily of the amino-terminal sequence and has a large fraction of organized secondary structure, while the β domain has a much higher fraction of coil conformation (Fig. 2*a*). Reduced and C199S mutant OxyR RD structures have the same fold, with no major differences in conformation. Discussion and comparison of the structures described here are based on the higher resolution C199S mutant structure as a proxy for the reduced OxyR RD.

The pairs of *P. gingivalis* OxyR RD monomers in the oxidized and C199S crystal asymmetric units are nearly identical in conformation (r.m.s.d.s of 0.58 and 0.52 Å, respectively). The largest differences between the oxidized and C199S *P. gingivalis* OxyR RD monomer conformations are in the segment from residues 190 to 223, which includes the disulfide loop. Different conformations in this segment observed in the *E. coli* OxyR RD structures were inferred to drive changes in quaternary structure (dimer and tetramer) and stability and to thereby determine the mode of DNA binding and control of the *E. coli* OxyR regulon. However, the local structural differences in *P. gingivalis* OxyR RD oxidized and C199S mutant forms do not match those observed for *E. coli* OxyR RD, which suggests that there are distinctions in the biological function of OxyR in these two biological species.

3.2. Disulfide-loop conformations

In *E. coli* the disulfide loop is approximately 15–20 Å from the dimer interface, close to the C-terminus of its monomer and almost antipodal to the amino-terminus, which connects to the DNA-binding domain. Comparison of the oxidized and C199S forms of *E. coli* OxyR RD showed that the switch between them (Fig. 3*b*) in response to oxidative stress or its absence causes local changes in polypeptide chain conformation. On oxidation (from left to right in Fig. 3*b*), there is a loss of the short α-helical turn in the disulfide loop and rearrangement of its conformation (*e.g.* Leu200). This is accompanied by a leftward shift (visualized relative to the background α-helix) of the upstream segment (*e.g.*

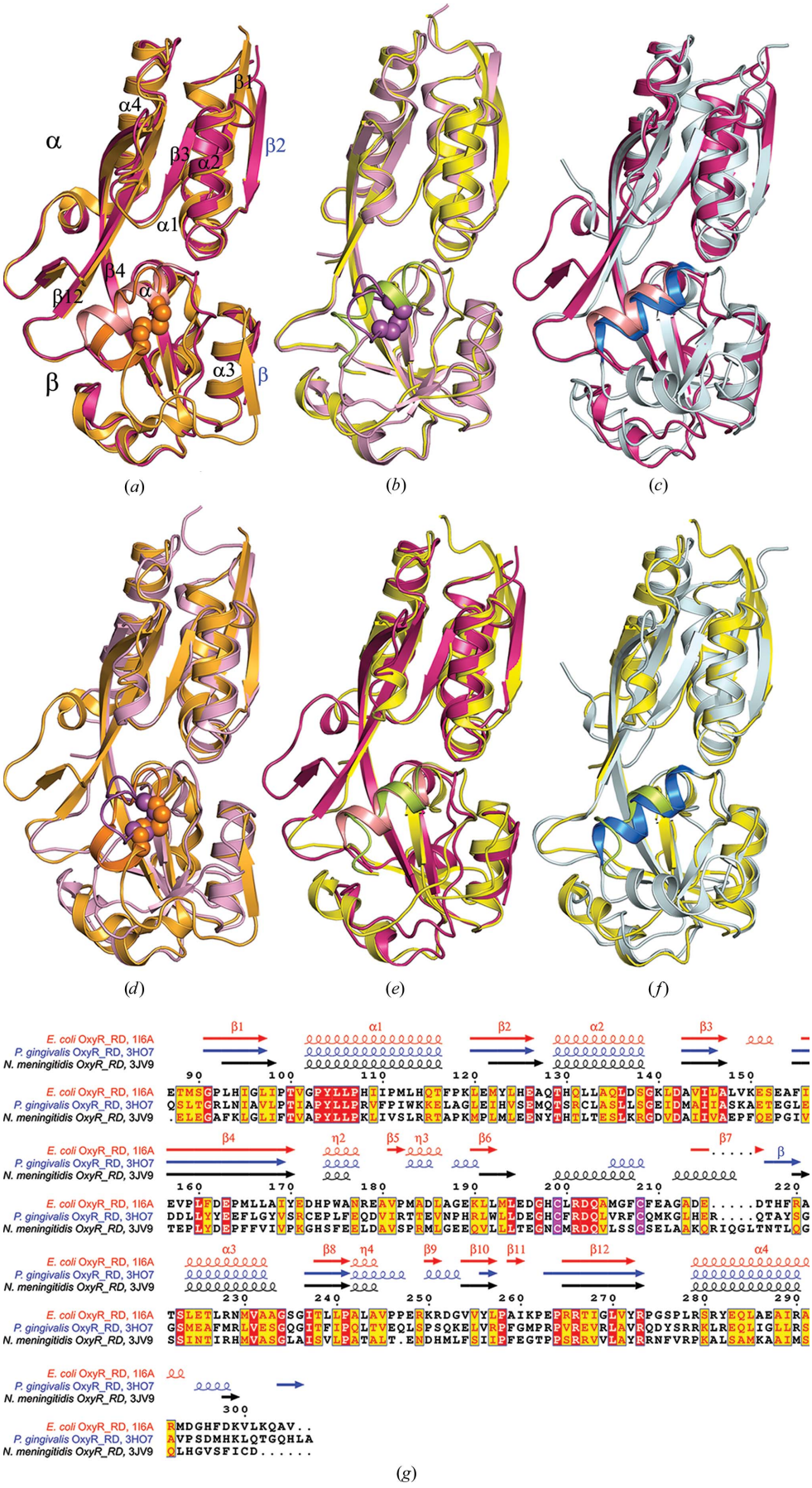

His198) away from the dimer interface on the right (not shown). These changes alter the dimer interface and were inferred to switch the quaternary-structure configuration and its mode of binding to the DNA promoter regions of the OxyR regulon.

The disulfide loops of oxidized and C199S *P. gingivalis* OxyR RD also differ significantly in conformation (right and left panels in Fig. 3*a*, respectively). Both lie in the same surface location on each monomer of the asymmetric unit as that in the counterpart structures for *E. coli*. Cys(Ser)199 and Cys208 in oxidized and C199S *P. gingivalis* OxyR RD coincide closely in position with those of the corresponding *E. coli* OxyR RD forms. However, the intervening disulfide-loop conformations of C199S and oxidized *P. gingivalis* OxyR RD differ significantly in conformation from their counterparts in *E. coli* OxyR RD despite their high sequence similarity (Figs. 3*a* and 3*b*, Table 2). The 199–208 segment in C199S *P. gingivalis* OxyR RD (Fig. 3*a*, left) is almost entirely α-helix, while

Figure 2
Pairwise structure and sequence alignment of OxyR RD homologues. C^{α} ribbon-diagram alignment of (*a*) C199S (red) and oxidized (orange) *P. gingivalis* OxyR RD monomer subunits (orange spheres are the disulfide-linked Cys199 and Cys208 in oxidized OxyR RD, and the α-helix of the Cys199–Cys208 disulfide loop in C199S mutant OxyR RD is shown in pink); (*b*) *E. coli* C199S OxyR RD (yellow with the Cys199–Cys208 disulfide loop highlighted in green) and oxidized form (magenta); (*c*) C199S (red) *P. gingivalis* and reduced (gray) *N. meningitidis* OxyR RD (the α-helix of the C199S mutant *P. gingivalis* OxyR RD disulfide loop is shown in pink and the α-helix of the reduced *N. meningitidis* OxyR RD disulfide loop is shown in blue); (*d*) oxidized *P. gingivalis* (orange) and *E. coli* (magenta) OxyR RD; (*e*) C199S *P. gingivalis* (red) and C199S *E. coli* (yellow) OxyR RD; and (*f*) C199S *E. coli* OxyR RD (yellow) and reduced *N. meningitidis* (gray) OxyR RD. (*g*) Sequence alignment of *E. coli*, *P. gingivalis* and *N. meningitidis* OxyR (see also Supplementary Fig. S2).

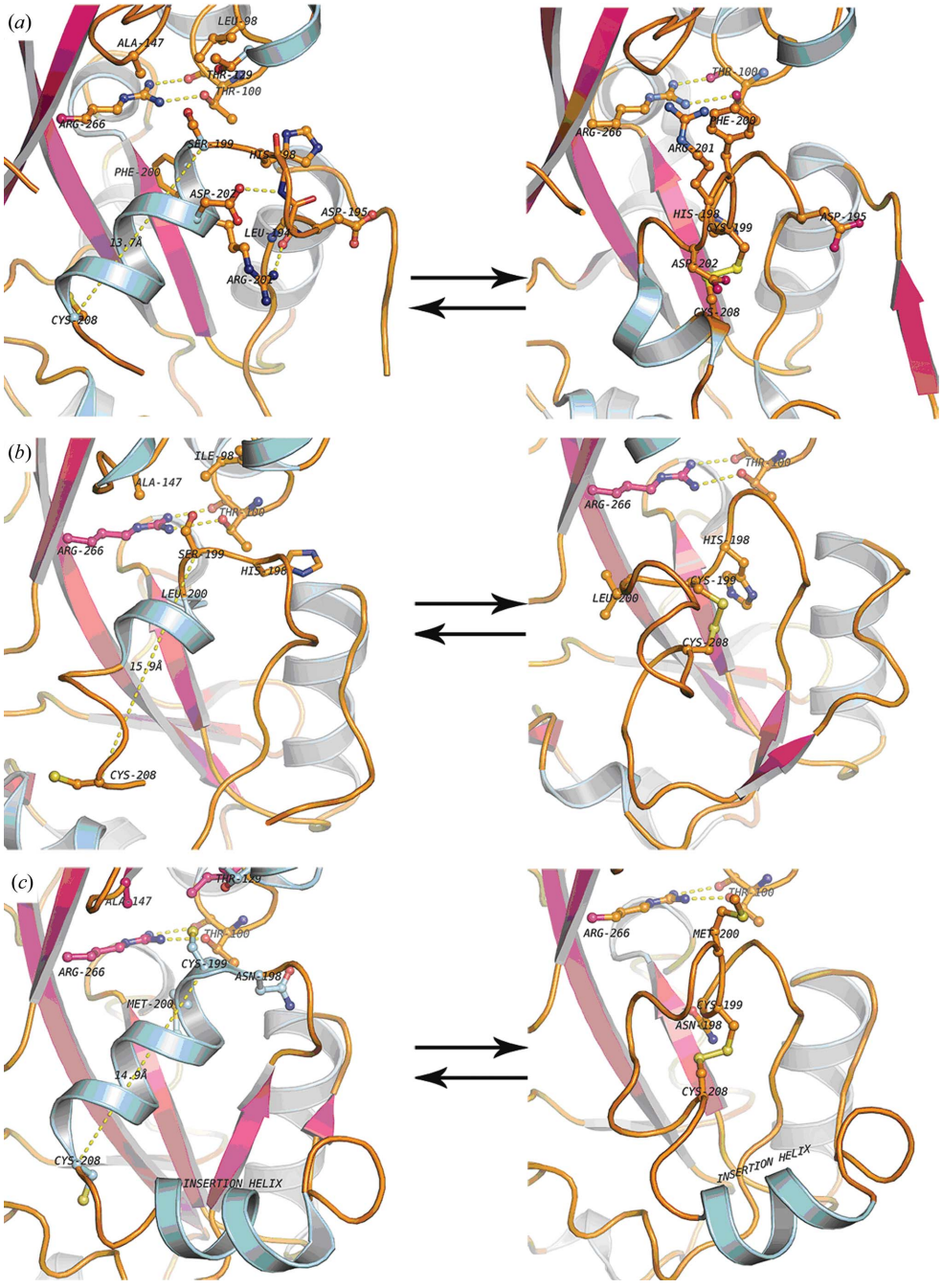

Figure 3
Reversible reduced–oxidized structural transitions around the disulfide loops of the three structurally characterized OxyR RDs. Reduced forms are in the left column and oxidized forms are in the right column. (*a*) *P. gingivalis* OxyR RD, (*b*) *E. coli* OxyR RD, (*c*) *N. meningitidis* OxyR RD (oxidized form modeled). The redox-active cysteines Cys(Ser)199 and Cys208 and some neighboring residues are shown in ball-and-stick representation. Yellow dashed lines show inferred hydrogen bonds and distances between the main-chain C^{α} atoms of Cys199/Ser199 and Cys208.

that of *E. coli* OxyR RD has only a single helical turn, with the remainder of the segment being in a coil conformation. The oxidized *E. coli* OxyR RD disulfide loop has essentially no α-helix, while oxidized *P. gingivalis* OxyR RD has about half the α-helix content of the C199S form (note the flip of Arg201; Fig. 3*a*), with the remainder being coil. In contrast to the oxidized and C199S forms of *E. coli* OxyR RD, this transition does not shift the segment upstream of residue 199 away from the dimer interface (Fig. 3*a*; note the unmoved Asp195). As a result, the juxtaposition of monomers in oxidized and C199S *P. gingivalis* OxyR RD is almost unchanged.

The disulfide loops of oxidized *E. coli* and *P. gingivalis* OxyR RD make relatively few polar interactions with the rest of the monomer and a comparable number of hydrophobic interactions. Of the six hydrogen bonds made by residues in the disulfide loop of oxidized *E. coli* OxyR RD, all but one are made to other residues within the loop segment, while four of the seven hydrogen bonds in the disulfide loop of oxidized *P. gingivalis* OxyR RD are made to residues internal to the loop segment and three to groups elsewhere in the monomer. The disulfide loop in oxidized *P. gingivalis* OxyR RD appears to be more tightly anchored to the rest of the OxyR RD structure than its *E. coli* OxyR RD counterpart.

In the C199S form of *P. gingivalis* OxyR RD residues Ser199 and Cys208 are 14 Å apart, close to that observed in the C199S form of *E. coli* OxyR RD (16 Å). Ser199 lies in the same surface pocket in the C199S mutant *P. gingivalis* OxyR RD (Fig. 3*a*) as observed for the C199S mutant *E. coli* OxyR RD structure (Fig. 3*b*). This pocket is more hydrophilic in C199S *P. gingivalis* OxyR RD than in *E. coli* OxyR RD and has a hydrogen-bonding network consisting of Arg266, Gln203, Ala147, Thr129, Thr100 and multiple water molecules. The side chain of Ser199 in the C199S mutant of *P. gingivalis* OxyR RD is directed towards the side chains of Leu98 and Ala147 and hydrogen bonds to a water molecule. This contrasts with *E. coli* C199S OxyR RD, where the pocket is more hydrophobic and is composed of the Leu200, Leu229 and Pro241 side chains (Choi *et al.*, 2001).

Arg266 within this pocket is conserved in the three OxyR RD structures from different bacterial species (Fig. 3). In all cases its guanidinium group makes multiple hydrogen bonds

Table 2
Secondary-structure differences between *P. gingivalis* and *E. coli* OxyR RD monomer structures and comparison of local r.m.s.d. differences between their oxidized and C199S mutant structures.

α, α-helix; β, β-strand; c, coil; T, turn.

P. gingivalis OxyR				*E. coli* OxyR			
Sequence	Mutant	R.m.s.d. (Å)	Oxidized	Oxidized	R.m.s.d. (Å)	Mutant	Sequence
148–153	c	0.22	c	α	0.20	α	149–153
190–192	β	0.09	c	β	0.32	c	190–192
199–210	α	2.77	c	c	3.79	c α c	199–210
211–216	N/A	N/A	c	c β	N/A	N/A	211–216
217–221	c β c	0.06	β	c	1.66	c	217–221
246–257	α	0.16	α	β T β	0.16	β T β	249–257
264–265	β	0.004	β	c	0.007	c	264–265

within the pocket and may therefore not contribute significantly to electrostatically neutralizing a putative cysteine sulfide or oxidized anion in this site (Kim *et al.*, 2002). While the polarity of this pocket differs among the three known C199S and reduced structures (hydrophobic in *E. coli* OxyR RD, electronegative in *P. gingivalis* and *N. meningitidis* OxyR RD), none offers a highly stabilizing environment for binding a cysteine anion. On the other side of the disulfide-loop switch, the Cys208 side chain of the C199S mutant *P. gingivalis* OxyR RD makes few interactions, and additional density at the S^{γ} atom indicates that the side chain may be partially in the oxidized sulfenic acid form. The immediately downstream Gln209 has weak density and residues 210–217 are not visible.

The local conformational differences between the oxidized and C199S *P. gingivalis* OxyR RD monomer are comparable in extent although distinct from those observed for the *E. coli* OxyR RD monomer. As a result, the conformational changes in *P. gingivalis* OxyR RD on oxidation/reduction are not propagated to the dimer interface in the same way and do not lead to large changes in quaternary structure as observed for *E. coli* OxyR RD.

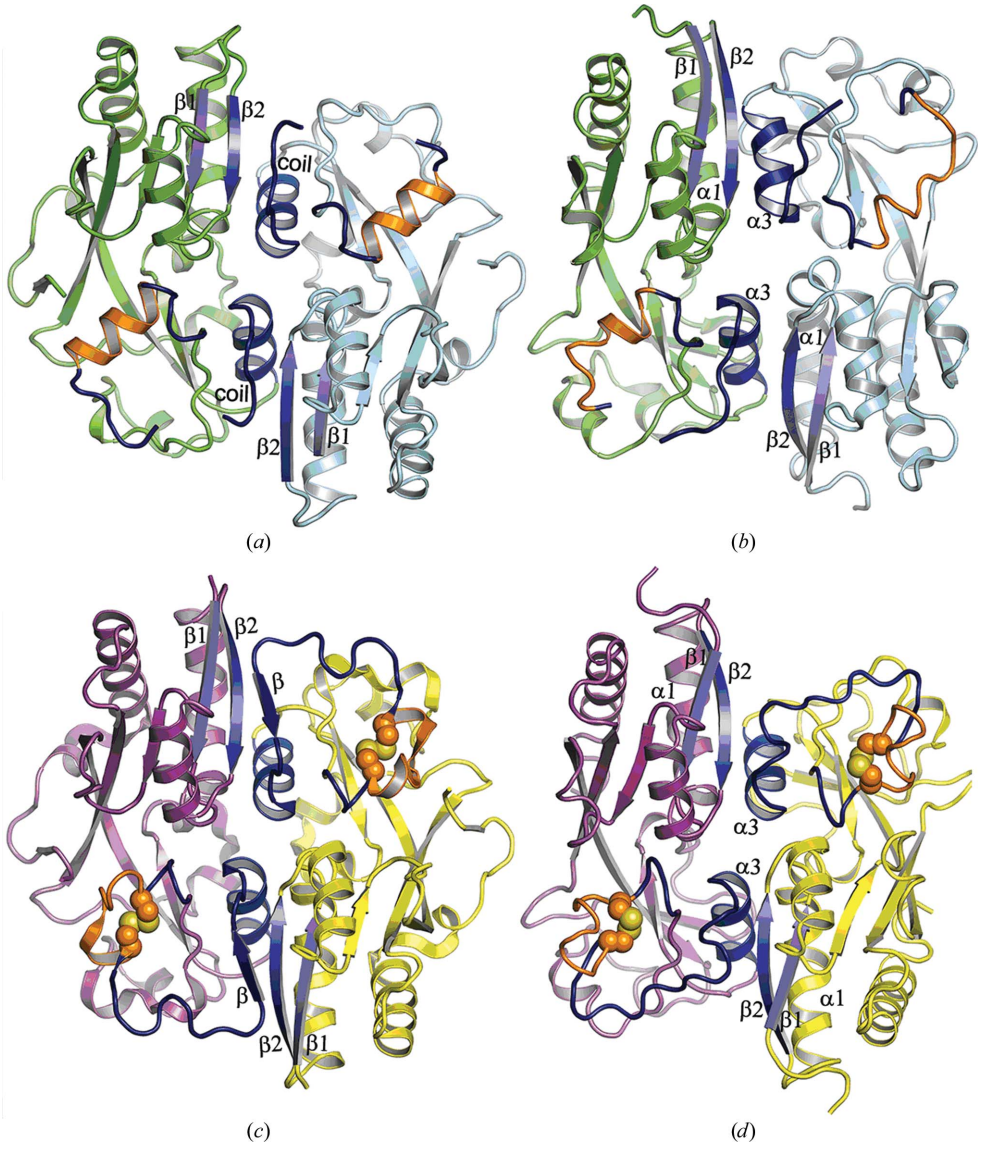

Figure 4
Dimer configurations of *P. gingivalis* and *E. coli* reduced and oxidized forms. (*a*, *c*) Reduced and oxidized dimers of *P. gingivalis* OxyR show no major changes in the relative orientation of monomers on oxidation/reduction; (*b*, *d*) reduced and oxidized dimers of *E. coli* OxyR showing relative rotational dislocation (30°) of monomers on oxidation/reduction.

3.3. Quaternary structures of oxidized and reduced *P. gingivalis* OxyR RD

The structural changes accompanying the transition between the C199S and oxidized disulfide-bridge forms of *E. coli* OxyR RD result in a relative rotation of 30° between the monomers of the dimer (Choi *et al.*, 2001; Figs. 4*b* and 4*d*), as measured by, for example, the relative orientation of the 102–117 (α1) and 225–234 (α3) α-helices on opposed monomers. These changes alter the monomer–monomer interface of the *E. coli* OxyR RD dimer, which in turn results in a major reorganization of the tetrameric (dimer of dimers) quaternary structure, and imply alterations in the disposition of the DNA-binding domains and in their promoter-binding specificities.

In contrast to *E. coli* OxyR RD, dimers of the oxidized and C199S forms of *P. gingivalis* OxyR RD have closely similar monomer orientations and interactions,

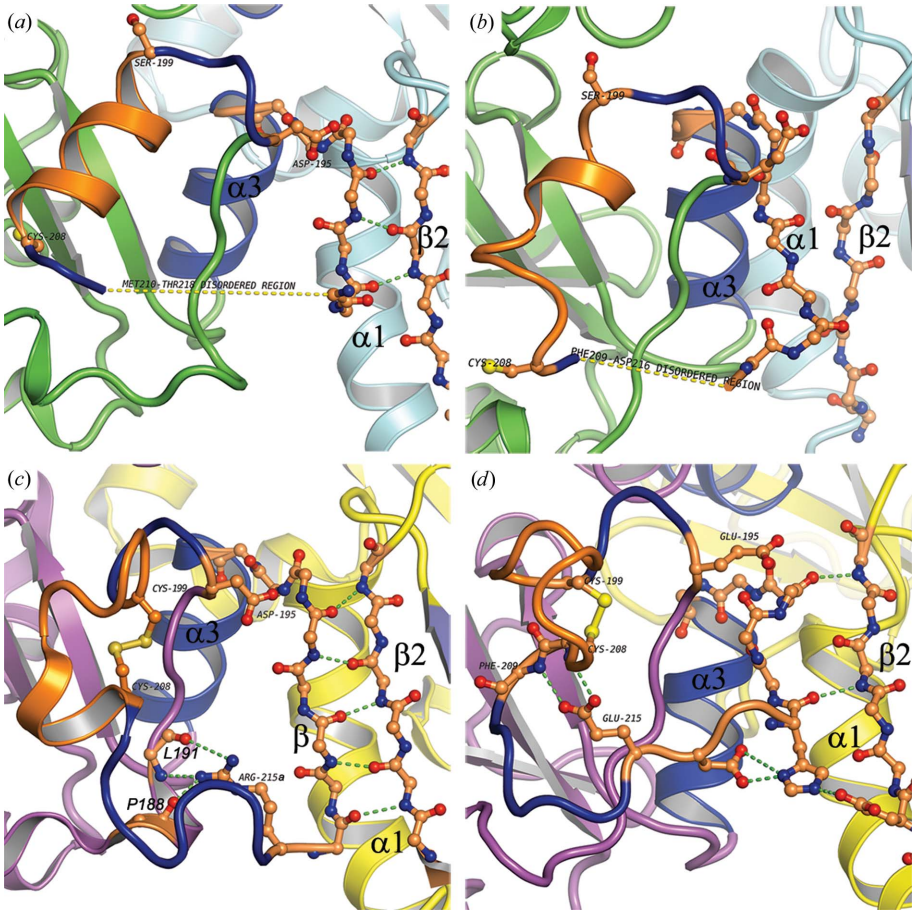

Figure 5
Dimer interface of *P. gingivalis* and *E. coli* OxyR in reduced and oxidized forms. (*a*, *b*) Reduced forms of *P. gingivalis* and *E. coli* OxyR showing opposed chains (ball-and-stick representation) at the interface of monomers; (*c*, *d*) oxidized forms of *P. gingivalis* and *E. coli* OxyR. Color coding and overall orientation is the same as in Fig. 3. Dashed green lines indicate a hydrogen-bonding network which is absent in the *E. coli* reduced dimer.

both resembling the oxidized dimer of *E. coli* OxyR RD (Figs. 4*a* and 4*c*). The change in quaternary structure between oxidized and C199S mutant forms observed in *E. coli* OxyR RD does not occur in the *P. gingivalis* OxyR RD dimer. In the latter the dimer juxtaposition is conserved and only minor dislocations near the interface are observed. The contact-surface areas for the oxidized *E. coli* and *P. gingivalis* dimers are 1168 and 1537 Å^2, respectively, and those for the C199S *E. coli* and *P. gingivalis* dimers are 973 and 1366 Å^2, respectively (calculated using *AREAIMOL* in *CCP*4 by taking the difference between the sum of the calculated surface areas of the individual subunits and those of the dimers). The more extensive contact surfaces of oxidized and C199S *P. gingivalis* OxyR RD relative to the corresponding *E. coli* dimers are consistent with a higher barrier to quaternary-structure change and greater dimer stability.

Detailed comparison of the C199S and oxidized structures of *P. gingivalis* OxyR RD shows that residues 217–221 in the oxidized form adopt a β-strand conformation that is part of a β-sheet across the dimer interface with residues 121–126 (β2) of the opposed monomer (Figs. 4*c* and 1*a*). This intermonomer β-sheet in oxidized *P. gingivalis* OxyR RD is unique among the known OxyR RD structures. In the C199S form this β-strand is distorted and shortened to residues 219–221 (coil), but still hydrogen bonds to β2 (residues 124–126) of the opposed monomer (Fig. 4*a*). The upstream contiguous segment 211–215a in oxidized *P. gingivalis* OxyR RD consists of ordered coil, but in the C199S form residues 211–218 are missing and disordered. The β2-strand segment from residues 120 to 126 is two residues longer in the oxidized than in the C199S form (121–125) of *P. gingivalis* OxyR RD and the β1 strand from 90 to 97, which pairs to the other side of β2 strand 120–126, is three residues longer than in the C199S form (93–97). Other stabilizing hydrophobic interactions involving α-helices α1 and α3, similar to those in the *E. coli* OxyR RD, also exist in both the oxidized and C199S *P. gingivalis* OxyR RD dimers.

Comparison of this region in oxidized and C199S *P. gingivalis* OxyR RD with that of oxidized and C199S *E. coli* OxyR RD shows that the 216–221 segment is in a pseudo-helical coil conformation in both oxidized and C199S *E. coli* OxyR RD. However, only the oxidized form shows intermonomer interactions (two hydrogen bonds in an imperfect β-sheet) with the β2 strand 121–126 of the opposed monomer. Residues 210–215 in C199S *E. coli* OxyR RD are disordered and are not visible in the electron density. A summary of the local structure differences between *E. coli* and *P. gingivalis* OxyR RD is given in Table 2.

3.4. Redox signal transmission from disulfide bridge to dimer interface

Comparison of the *E. coli* and *P. gingivalis* OxyR RD structures shows how the pathways of structural change from the disulfide switch to the monomer–monomer interfaces of the respective dimers diverge. In *E. coli*, breakage of the Cys199–Cys208 disulfide bridge in oxidized OxyR RD displaces Glu215, which hydrogen bonds to the –NH– groups of Cys208 and Phe209 (Fig. 5*d*). Glu215 lies in the critical β7 (214–216) strand of the two-strand β-sheet consisting of β6 and β7 and its displacement disrupts this β-sheet interaction. As a result the 216–221 pseudo-helical segment at the monomer–monomer interface is released, changing its conformation and inducing disorder in the residues immediately upstream (210–215) in the C199S mutant form (Fig. 5*b*). These changes are likely to contribute to lowering the energy barrier to reorganization of the monomer–monomer interface

in the oxidized↔reduced conversion of *E. coli* OxyR and to favor the switch to the more stable reduced dimer configuration.

In contrast to *E. coli* OxyR RD, Glu215 in oxidized *P. gingivalis* OxyR RD extends into solution and does not hydrogen bond with Cys208, which instead forms hydrogen bonds with Leu204 within the disulfide loop. The insertion of Arg215a (Fig. 2*g*) in *P. gingivalis* OxyR (Fig. 5*c*) relative to the *E. coli* OxyR sequence extends 216–221 farther towards β2 strand 122–126 of the opposing monomer of the dimer than occurs in C199S *E. coli* OxyR RD. The side chain of Arg215a in oxidized *P. gingivalis* OxyR RD faces inwards and its guanidinium group is locked by hydrogen bonds between the carbonyl O atoms of Leu191 and Pro188 (Fig. 5*c*). The extension conferred by the single stabilizing Arg215a insertion in *P. gingivalis* OxyR RD permits residues 216–221 to form the intermonomer β-sheet with β2 (122–126) of the opposing monomer. This latter β2 strand is paired with β1 (90–97) of its own monomer in both the oxidized and reduced forms and thus a three-strand intermonomer β-sheet exists in *P. gingivalis* OxyR RD. Reduction of the disulfide link in *P. gingivalis* OxyR and changes in the disulfide-loop conformation disrupt the Arg215a side-chain hydrogen bonding, with consequent disordering of the 210–215 segment and some limited distortion of the β conformation in the 216–221 segment (Fig. 5*a*). This latter reduces the number of hydrogen bonds between the monomers to three in the C199S mutant form from five in the oxidized form. These structural features, along with the disruption of the Arg215a side-chain hydrogen bonds and the disordering of the 210–216 segment, suggest that the C199S mutant and oxidized forms of *P. gingivalis* OxyR RD may have comparable thermodynamic stability, in contrast to *E. coli* OxyR RD, where the reduced form is more stable than the oxidized form.

3.5. An important structural role for the sequence insert at residue 215

The arginine (215a) insertion at residue 215 in *P. gingivalis* OxyR RD, as noted above, appears to be important in stabilizing the monomer–monomer interactions of *P. gingivalis* OxyR in the oxidized configuration first observed in *E. coli* OxyR RD. *N. meningitidis* OxyR has a five-residue insertion at residue 215, including an arginine at 215a (Figs. 2*e* and 3*c*), and a structure has been determined for its reduced form (Sainsbury *et al.*, 2010). This structure has a closely similar monomer fold to that of *E. coli* and *P. gingivalis* OxyR RD (Fig. 2*c*) and the crystal dimer of reduced *N. meningitidis* OxyR RD has the same configuration as reduced *E. coli* OxyR RD.

However, the local conformation around residue 215 and the stabilizing intermonomer interactions in *N. meningitidis* OxyR RD are different from those in *P. gingivalis* and *E. coli* OxyR RD. Arg215a in *N. meningitidis* OxyR RD is exposed to solvent and does not directly affect the intermonomer interactions that are important for stabilizing the dimer of *P. gingivalis* OxyR RD. However, the 211–219 α-helix in *N. meningitidis* OxyR RD centered on the five-residue sequence insertion at 215 creates an alternative set of monomer–monomer interactions distinct from those of *P. gingivalis* OxyR RD; these appear to stabilize the *N. meningitidis* OxyR RD in its reduced dimer configuration. There is no intermonomer β-sheet interaction like that observed in *P. gingivalis* OxyR RD, but the reduced *N. meningitidis* OxyR RD dimer is extensively stabilized by intermonomer hydrophobic interactions of helix α1 (225–238) with helix α3 (102–117) and strand β2 (121–127). There are also hydrogen bonds between the monomers: the side-chain –OH of Ser238 (3.0 Å) with the main chain –NH– of Leu122, the Ser228 side-chain hydroxyl with the Glu126 (2.5 Å) side-chain O atom, and the carbonyl O atom of Met256 with the guanidine group of Arg114 (3.0 Å). None of these occur in the *E. coli* OxyR RD dimers. The reduced *N. meningitidis* OxyR RD also has a much larger intermonomer surface area (1429 Å^2) than the reduced *E. coli* dimer (973 Å^2).

3.6. Modeling of full-length OxyR oligomers and their complexes with DNA

The binding of LysR transcriptional regulators to their DNA operator regions has been shown in most cases to involve the tetramerization of pre-bound dimers with consequent stabilization of bent DNA (Maddocks & Oyston, 2008). For *E. coli* OxyR it has been proposed (Choi *et al.*, 2001), based on the tetrameric structure of C199S *E. coli* OxyR RD, that the redox switch drives the oxidized↔reduced transition between two different modes of tetramer binding to the DNA promoter region: activator (oxidized) and repressor (reduced). Protection experiments (Toledano *et al.*, 1994) show that in the activator mode the oxidized tetramer binds, presumably in its closed form, to around four consecutive turns of DNA helix. In contrast, the reduced (putatively open) repressor form binds to around five turns of DNA helix, with the central turn not being involved in DNA recognition. The latter is inferred to be permissive for binding to a bent DNA that cannot be transcribed from its promoter, while the former cannot adopt this repressive bent DNA complex conformation but can interact with RNA polymerase to activate transcription.

In the absence of structural information for full-length *P. gingivalis* or any other OxyR, we used homology modeling based on known LysR tetramer structures, as was performed for the reduced *N. meningitidis* full-length OxyR model (Sainsbury *et al.*, 2010). Modeling of full-length tetramers by the superposition of the dimers of known structure on the tetramer template showed no major overlap at the inter-dimer interfaces for the reduced closed *P. gingivalis* OxyR tetramer, but oxidized tetramers could not be built. Similarly, for *N. meningitidis* OxyR major overlap of the 199–221 region in our modeled oxidized dimers prevented oxidized tetramers from forming, but a reduced open tetramer could be built (top row of Fig. 6).

To test which DNA-bound oligomers of full-length *P. gingivalis* OxyR are structurally possible, we modeled full-length *P. gingivalis* OxyR dimers and tetramers using the

CbnR (PDB entry 1iz1) and TtgV (PDB entries 2xrn and 2xro) structures as templates, respectively (Fig. 7). We strictly conserved the *P. gingivalis* OxyR RD dimer structures and monitored dimer–dimer and tetramer–DNA clashes. Oxidized *P. gingivalis* OxyR cannot be modeled based on CbnR as either an open or a closed LysR-type tetramer in the DNA-bound state because of clashes in the Cys199–Cys208 switch region. C199S *P. gingivalis* OxyR, which differs in its disulfide-loop conformation from the oxidized form, but whose regulatory domain dimer configuration is closely similar to the oxidized form, can be modeled bound to DNA as a closed tetramer only (bottom row of Fig. 6). These modeling results are summarized in Fig. 6 and predict the binding of *P. gingivalis* oxidized OxyR to its promoter region in the oxidized dimer configuration with activation of transcription; reduced OxyR is predicted to bind as a closed tetramer composed of two reduced dimers in the oxidized dimer configuration and to also activate transcription. A number of *P. gingivalis* OSR genes are constitutively activated and none are de-repressed under H_2O_2 stress or in a knockout-mutant OxyR strain (Diaz *et al.*, 2006). We suggest that the constitutive activation of these genes in *P. gingivalis* is mediated under anaerobic reducing conditions by the closed tetramer (two reduced dimers in the oxidized dimer configuration) and that under (transient) oxidizing aerobic conditions dimers of oxidized OxyR maintain the activation of these OSR genes. These modeling results explain how oxidized and reduced OxyR can both be activators of transcription. Conversely, reduced *N. meningitidis* OxyR is predicted from model building to bind its promoter in the reduced dimer configuration and oxidized *N. meningitidis* OxyR is predicted to bind as a tetramer of two oxidized dimers in the reduced configuration as an open tetramer. Gene-expression data for *N. meningitidis* are sparse, but our results raise the possibility that its OxyR represses transcription under both oxidizing and reducing conditions.

These models can at best identify those OxyR–DNA complexes that are not possible. This exclusionary procedure derives from two structural determinants of the oligomeric state of DNA-bound OxyR. Firstly, sequence and local conformational differences in the contact surfaces of subunits affect the possible dimer and tetramer configurations and their stable complexes with DNA. Secondly, differences in the conformation of the disulfide loops among the three species and between oxidized and reduced forms affect protein–protein and protein–DNA interactions. The modeling of *P. gingivalis* and *N. meningitidis* OxyR–DNA complexes, both of which have an insert at residue 215, reveals similar patterns of permitted DNA-bound oligomeric forms, but with the

	Ec_{ox}		Ec_{red}		Pg_{ox}		Pg_{red}		Nm_{ox}		Nm_{red}	
	2	4	2	4	2	4	2	4	2	4	2	4
−DNA	▲	↻	▼	⇄	▲	↻	▲	↻	▼	⇄	▼	⇄
+DNA	▲	↻	▼	⇄	▲	×	×	↻	▼	×	×	⇄

×, cannot form; ▲, oxidized dimer configuration; ▼ reduced dimer configuration; ↻, closed tetramer only; ⇄, open tetramer only.

Figure 6
Summary of predicted full-length OxyR dimer (2) and tetramer (4) forms and their DNA complexes from structure-based model building. The exclusion of structures based on unfavorable OxyR–OxyR and OxyR–DNA contacts leaves a unique set of OxyR forms (dimer, tetramer; oxidized, reduced; open, closed) for each of the three species. Ec, *E. coli*; Pg, *P. gingivalis*; Nm, *N. meningitidis*.

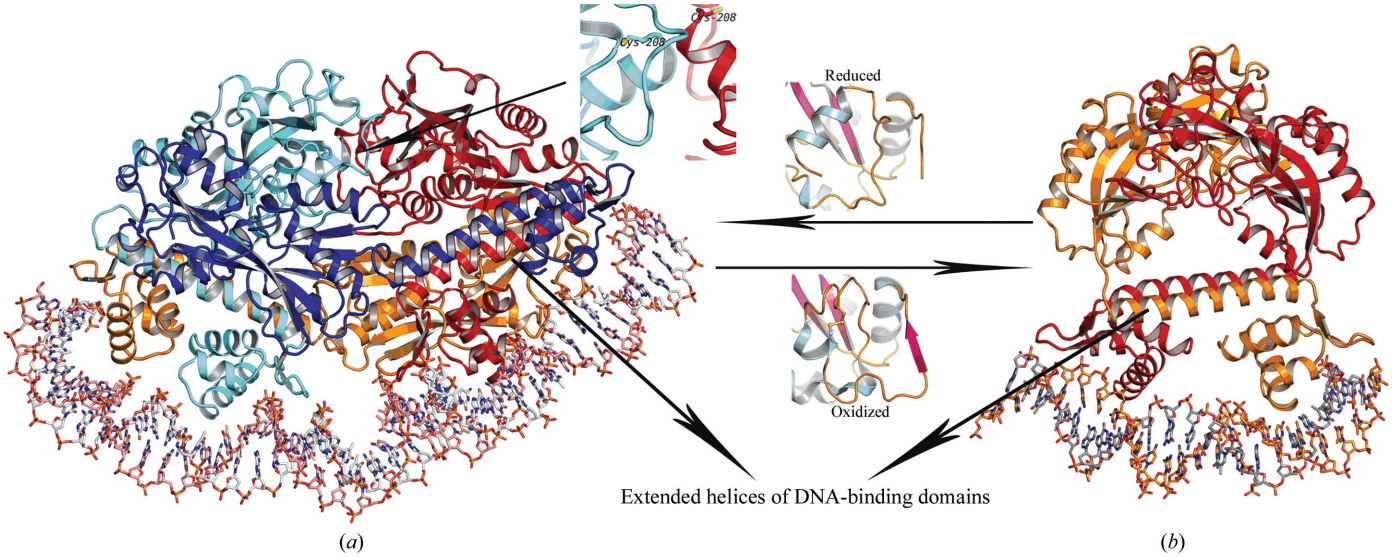

Figure 7
Full-length OxyR–DNA complex models. Modeled structures of reduced (left) *P. gingivalis* OxyR closed tetramer and oxidized (right) dimer bound to DNA. (*a*) Tetramer (monomer chains color-coded blue, cyan, orange and red) of reduced dimers (cyan with blue and orange with red). These are stabilized by interactions between extended helices of DNA-binding domains (lower left arrow) from a monomer of each dimer (blue with red and orange with cyan) and by interaction of Cys199–Cys208 α-helices between regulatory domains (cyan with red and blue with orange; upper left arrow); (*b*) oxidized dimer, formed through hydrophobic interactions between extended helices (lower right arrow) in DNA-binding domains, bound to two turns of DNA. Middle arrows indicate the reversible transition from reduced tetramer (left) to oxidized dimer (right).

reduced and oxidized dimers and the open and closed tetramers switched (Fig. 6). This is consistent with a structural and functional discriminant role for the residue 215 insert relative to *E. coli* OxyR and may reflect an adaptation that confers constitutive activation or repression in different bacterial OxyR regulons under both oxidizing and reducing conditions.

4. Discussion

Comparison of OxyR sequences and the existing structures of OxyR RD leads us to suggest that the presence of the sequence insert at residue 215 relative to *E. coli* OxyR is associated with OxyRs whose biological regulatory functions are distinct from those of *E. coli* OxyR. In the case of *P. gingivalis* OxyR RD, the insertion of Arg215 is important in maintaining closely similar dimer configurations in the oxidized and reduced forms. In *E. coli* OxyR, the switch between oxidized and reduced disulfide changes the dimer configuration and consequently also the tetramer structure. This results in an OxyR population that shifts rapidly in response to capricious changes in the oxidative environment and in which both oxidized and reduced tetramers are functional as activators or repressors, respectively. In contrast, the cysteine-disulfide redox switch in *P. gingivalis*, and we suggest also in *N. meningitidis* OxyR, appears to be uncoupled from quaternary-structure changes and the OxyR RD dimers in either redox state are locked in the activated (oxidized) and repressed (reduced) configuration, respectively. In the case of *P. gingivalis* OxyR, these locked dimers and the distinct conformation of the disulfide loop constrain the population of oligomers to activator forms (dimers, closed tetramers), based on modeling the DNA-free or DNA-bound forms. This is consistent with the constitutive expression of the OSR genes in *P. gingivalis* and their weak or absent induction in the presence of H_2O_2.

The functional variation in OxyR implied by relatively small differences in sequence and structure among *E. coli*, *P. gingivalis* and *N. meningitidis* OxyR may reflect adaptation to distinct selective pressures. However, the absence of a switch in gene expression on switching of the redox state of the sensor disulfide raises the question of why the latter is present. OxyR may have a wide diversity of regulons and also different sensor functions that may extend beyond that of the redox (peroxide) sensing cysteine-disulfide switch. Other sensor functions for the redox cysteines of OxyR have been inferred from observations that under certain conditions Cys199 in *E. coli* OxyR forms sulfenic acid, *S*-nitrosyl and glutathionyl adducts that appear to change the conformational properties of the OxyR (Kim *et al.*, 2002). While these results have not been completely reconciled with the other extensive studies establishing the role of the OxyR disulfide switch in the response of *E. coli* to peroxide stress, they suggest a more extensive panel of other regulatory roles for OxyR than that inferred for *E. coli*. Recently, it was shown that nitrosylation of OxyR Cys199 occurs in *E. coli* grown under anaerobic conditions and that OxyR controls expression of a nitrosative stress regulon distinct from the oxidative stress regulon (Seth *et al.*, 2012). The case of the two *D. radiodurans* OxyR alleles, both of which lack Cys199 and the insert at 215, but which regulate some OSR genes on H_2O_2 challenge (Chen *et al.*, 2008), points to regulatory functions of OxyR that do not utilize the cysteine-disulfide redox switch. The case of *P. gingivalis* OxyR RD described here shows that OxyR can retain transcriptional activation activity in both oxidized and reduced forms as a result of very limited changes in its sequence and structure. This apparent loss of regulatory discrimination may permit an expanded range of other OxyR regulatory functions.

We thank Dr Faik Musayev for help with data collection, Dr Neel Scarsdale for useful advice during structure determination and refinement, Ms Cecilia Anaya and Ms Sai Yanamandra for help with protein purification, Ms Dipanwita Sengupta for help with the C199S mutant construction and Cynthia Cornelissen for useful discussion. This work was supported by grants from National Institutes of Health (Nos. R01DE018039 and 3R01DE018039-S1 to JPL) and National Institutes of Health (No. CA 16059-28) to the Massey Cancer Center in support of the structural biology resources used in this study.

References

Adams, P. D. *et al.* (2010). *Acta Cryst.* D**66**, 213–221.
Antelmann, H. & Helmann, J. D. (2011). *Antioxid. Redox Signal.* **14**, 1049–1063.
Arnold, K., Bordoli, L., Kopp, J. & Schwede, T. (2006). *Bioinformatics*, **22**, 195–201.
Chen, H., Xu, G., Zhao, Y., Tian, B., Lu, H., Yu, X., Xu, Z., Ying, N., Hu, S. & Hua, Y. (2008). *PLoS One*, **3**, e1602.
Choi, H., Kim, S., Mukhopadhyay, P., Cho, S., Woo, J., Storz, G. & Ryu, S. E. (2001). *Cell*, **105**, 103–113.
Diaz, P. I., Slakeski, N., Reynolds, E. C., Morona, R., Rogers, A. H. & Kolenbrander, P. E. (2006). *J. Bacteriol.* **188**, 2454–2462.
Emsley, P. & Cowtan, K. (2004). *Acta Cryst.* D**60**, 2126–2132.
Fareleira, P., Santos, B. S., Antonio, C., Moradas-Ferreira, P., LeGall, J., Xavier, A. V. & Santos, H. (2003). *Microbiology*, **149**, 1513–1522.
Honma, K., Mishima, E., Inagaki, S. & Sharma, A. (2009). *Microbiology*, **155**, 1912–1922.
Imlay, J. A. (2002). *Adv. Microb. Physiol.* **46**, 111–153.
Imlay, J. A. (2008). *Annu. Rev. Biochem.* **77**, 755–776.
Kiefer, F., Arnold, K., Künzli, M., Bordoli, L. & Schwede, T. (2009). *Nucleic Acids Res.* **37**, D387–D392.
Kim, S. O., Merchant, K., Nudelman, R., Beyer, W. F., Keng, T., DeAngelo, J., Hausladen, A. & Stamler, J. S. (2002). *Cell*, **109**, 383–396.
Lee, C., Lee, S. M., Mukhopadhyay, P., Kim, S. J., Lee, S. C., Ahn, W.-S., Yu, M.-H., Storz, G. & Ryu, S. E. (2004). *Nature Struct. Mol. Biol.* **11**, 1179–1185.
Lu, D., Fillet, S., Meng, C., Alguel, Y., Kloppsteck, P., Bergeron, J., Krell, T., Gallegos, M. T., Ramos, J. & Zhang, X. (2010). *Genes Dev.* **24**, 2556–2565.
Maddocks, S. E. & Oyston, P. C. F. (2008). *Microbiology*, **154**, 3609–3623.
Meuric, V., Gracieux, P., Tamanai-Shacoori, Z., Perez-Chaparro, J. & Bonnaure-Mallet, M. (2008). *Oral Microbiol. Immunol.* **23**, 308–314.
Monferrer, D., Tralau, T., Kertesz, M. A., Dix, I., Solà, M. & Usón, I. (2010). *Mol. Microbiol.* **75**, 1199–1214.
Muraoka, S., Okumura, R., Ogawa, N., Nonaka, T., Miyashita, K. & Senda, T. (2003). *J. Mol. Biol.* **328**, 555–566.

Murshudov, G. N., Skubák, P., Lebedev, A. A., Pannu, N. S., Steiner, R. A., Nicholls, R. A., Winn, M. D., Long, F. & Vagin, A. A. (2011). *Acta Cryst.* D**67**, 355–367.
Ohara, N., Kikuchi, Y., Shoji, M., Naito, M. & Nakayama, K. (2006). *Microbiology*, **152**, 955–966.
Peitsch, M. C. (1995). *Biotechnology*, **13**, 658–660.
Ryu, S. E. (2012). *J. Biochem.* **151**, 579–588.
Sainsbury, S., Ren, J., Nettleship, J. E., Saunders, N. J., Stuart, D. I. & Owens, R. J. (2010). *BMC Struct. Biol.* **10**, 10.
Seth, D., Hausladen, A., Wang, Y.-J. & Stamler, J. S. (2012). *Science*, **336**, 470–473.
Storz, G. & Imlay, J. A. (1999). *Curr. Opin. Microbiol.* **2**, 188–194.
Toledano, M. B., Kullik, I., Trinh, F., Baird, P. T., Schneider, T. D. & Storz, G. (1994). *Cell*, **78**, 897–909.
Wu, J., Lin, X. & Xie, H. (2008). *FEMS Microbiol. Lett.* **282**, 188–195.
Zheng, M., Wang, X., Templeton, L. J., Smulski, D. R., LaRossa, R. A. & Storz, G. (2001). *J. Bacteriol.* **183**, 4562–4570.